Journal of Metals, Materials and Minerals, Vol. 32, No. 2, pp. 1-10, 2022

The Structure and ferromagnetism of carbon nanofibers from polyacrylonitrile/ polyvinylpyrrolidone

Suminya TEETA[1], Ratchaneekorn WANCHANTHUEK[2], Somchai SONSUPAP[3], Santi MAENSIRI[3], Narong CHANLEK[4], and Kwanruthai WONGSAPROM[1,*]

[1] *Physical Materials Science Unit Research, Department of Physics, Faculty of Science, Mahasarakham University, Mahasarakham 44150, Thailand*
[2] *Department of Chemistry, Faculty of Science, Mahasarakham University, Mahasarakham 44150, Thailand*
[3] *SUT Center of Excellence on Advanced Functional Materials, Suranaree University of Technology, Nakhon Ratchasima 30000, Thailand*
[4] *Synchrotron Light Research Institute (SLRI), Nakhon Ratchasima 30000, Thailand*

***Corresponding author e-mail:** wkwanruthai@gmail.com

Received date:
7 September 2021
Revised date
21 February 2022
Accepted date:
16 March 2022

Keywords:
Electrospinning;
Ferromagnetic carbon;
Magnetic;
Nanofiber;
Polymer

Abstract

Room-temperature ferromagnetism was successfully induced in carbon. Carbon nanofibers were fabricated using sequential electrospinning of polyacrylonitrile (PAN) and polyvinylpyrrolidone (PVP). The morphologies, crystal structures, chemical bonding states and magnetic properties were characterized over three different weight ratios which were 10:0, 7:3 and 6:4 of PAN/PVP. The carbon nanofibers obtained after pyrolysis of polymer fibers were placed inside a tube furnace using a three steps process: stabilization, carbonization, and activation at 800°C. XRD patterns indicated the amorphous structure of carbon. The average diameter of the carbon nanofibers was between 340 nm to 511 nm. Raman analysis was used to determine the carbon qualities in the samples by the numbers of sp^3/sp^2 hybridized atoms. The chemical analysis obtained XPS indicated that there were no magnetic contaminants. The PAN/PVP weight ratio of 6:4 showed ferromagnetic carbon nanofibers with the highest specific saturation magnetization as ~144.2 m-emu·g^{-1} at 300 K. This indicated that the mixing of sp^2-sp^3 carbon system had localized magnetic moments. This finding suggests an inexpensive method for preparing magnetic particles and human-friendly ways to produce magnetic material without metals. These results inspire us to further research on the potential of carbon materials, as a completely new class of magnetic devices.

1. Introduction

The origin of magnetism in conventional ferromagnetic materials that are composed of metal elements is due to the presence of cations with partially filled *d* or *f* shells, such as iron, nickel and cobalt [1]. Ferromagnetic material can be used in many applications, including memory devices such as magnetic tapes, magnetic hard drives, and magnetic random-access memory, information (magnetic recording), magnetic shielding and magnetic recording permanent magnets, electromagnets core of the transformer magnetic tapes and memory stores [2]. There are recent reports of ferromagnetism in carbon materials, in which the ground state electronic configuration is $1s^2\ 2s^2\ 2p^2$. Generally, carbon systems cannot generate localized magnetic moments, in contrast to traditional ferromagnets. So, studying magnetism in carbon is an interesting at both fundamental and applied levels. Carbon-based materials are included in the list of ferromagnetic elements that contains only *s* and *p* electrons in contrast to traditional ferromagnets [3]. Magnetism of carbon-based material has been attracting great interest due to high temperature ferromagnetic behavior and applications. Conventional, carbon-based structures were initially believed to be diamagnetic or, in special cases, paramagnetic [4]. Ferromagnetism in carbon exhibiting spontaneous magnetization at room-temperature was reported as early as 1987 [5]. There have been a number of publications in which reproducible observations of room-temperature magnetic ordering in different carbon allotropes, such as graphite [6-9], graphene [10], proton-irradiated highly oriented pyrolytic graphite (HOPG) [6,11-12], carbon nanotubes [13-15], polymerized fullerenes [16], carbon nanofoam [17] and amorphous carbon [18] were reported. In addition, Ma *et al*. [19] suggested the observation of room temperature ferromagnetism in a polymer which includes Teflon tape subjected to simple mechanical stretching, heating, or cutting. Several reports have been published describing magnetism observed in carbon systems. The magnetic moments produced in carbon materials are suspected to be due to the existence of defects [6,20]. For example, hydrogen passivated zigzag and armchair edges [21]; carbon dangling bonds or vacancy-interstitial complexes [3,19], adatom defects [22-23] and hydrogen adsorption defects [24] were predicted to induce local magnetic moments and magnetic order in graphite or graphene [12]. The ferromagnetism in graphitic materials has been attributed to lattice imperfections. The induction of ferromagnetism was demonstrated in proton-irradiated graphite spots [11]. The pyrolytic graphite contained a high defect concentration showing increased magnetic signals [25]. Makarova and Palacio [24] reported that a major essential

for magnetism in an all-carbon structure is the presence and stability of carbon radicals. Radicals can introduce an unpaired spin and can bring down the potent susceptibility of pairing of all valence electrons in covalent bonds. However, the mechanism of ferromagnetism in pure carbon remains unclear [21]. Since Ovchinnikov and Spector [26] prepared ferromagnetic carbon material from polyacrylonitrile, many scientists have attempted the difficult task of reproducing ferromagnetic carbon materials. There have recently been several reports of weak ferromagnetism in carbon [27-29], since Liu *et al*. reported that carbon nanosheets with an amorphous structure and crystallized graphene nanocrystals inside exhibit ferromagnetic coupling with a yield saturation magnetization of 0.22 emu·g^{-1}, showing that the magnetic properties of carbon were dominated by the distance between zigzag edges. Meanwhile, Barrag´ *et al.* report that bamboo pyroligneous acid-derived oxidized graphene nanoplatelets exhibit ferromagnetic order at room temperature. The magnetization saturation was found to range from 2 m-emu·g^{-1} to 40 m-emu·g^{-1}, possibly induced by increased defect density as controlled by carbonization temperature, which leads to increased magnetization. In general, CNFs have great potential for applications utilizing their unique mechanical, electrical, and magnetic properties, as well as high surface area to volume ratio. For application, if it is technologically feasible to produce a bulk carbon magnetic material in gram amounts, it would be expected that they would be applicable to a wide field of modern technology for medical devices; adaptable, lightweight, and flexible information storage systems; have low production cost, molding capability, environmental friendliness, and biocompatibility. Biotechnology applications may include biosensors, targeted drug delivery, artificial muscles, magnetic buckles, magnetic markers, and magnetic resonance imaging [29-32]. For biomedical applications of magnetic behavior, such as target drug delivery, to diminish its toxicity in humans, the concept of magnetic drug delivery is to use an external magnetic field to propel a drug carrier with magnetic properties to a specific location in the body. A magnetic field enables controllable magnetic guidance and release, allowing drug delivery to tumor cells while avoiding damage to healthy tissue. Magnetic moment orientation in a material is the key to identifying different magnetism behaviors [33,34]. Recent reports describe the utilization of ferromagnetism in carbon materials in several applications as toner for copiers and other business machines, or as magnetic ink. The strong carbon magnets free from transition metals used as a brief scan of some of the patents. Magnetic resonance imaging could be improved by injecting the small ferro-magnetic clusters into blood arteries [35].

Carbon nanofibers have been attractive because of their specific thermal, morphological, electrical, mechanical properties and application. There are many methods for the synthesis of carbon nanofibers but generally, they have been synthesized by methods such as ion beam irradiation, electrospinning, catalytic chemical vapor deposition and a polymer blend technique, [29] etc. Among all the methods for the synthesis of CNFs, electrospinning is the most effective, facile, and low-cost technique. The polymer nanofibers were used as the precursor to the CNFs. There are several polymer precursors used to produce carbon nanofibers, e.g., polyacrylonitrile (PAN), polyvinylpyrrolidone (PVP), polyvinyl alcohol (PVA), polymethyl methacrylate (PMMA), polyimides (PIs) and so on. PAN is the most commonly used polymer, mainly due to its high carbon yield and flexibility. The carbon nanofiber was synthesized via electrospinning and a subsequent heat- treatment process. The mains steps of the heat-treatment process consist of stabilization and carbonization. Stabilization is used to convert the linear polymer into a ladder structure and crosslink the chain molecules and this can prevent the fibers from melting or fusing during higher temperature heat treatment. The carbonization process could be applied for removal of non-carbon material under an inert gas atmosphere. Activation is the process to increase the surface area of a carbonized organic precursor. Carbon nanofibers with large surface area can be expressed as a three-dimensional random network of nano-graphitic domains with particular dimensions of several nanometers. Jia Hao *et al.* [30] reported that the edge states in nanographite disordered network control its magnetic properties.

Usually, the fabrication of carbon fiber is achieved by electro-spinning using a polymer blend solution to create porous fibers after the volatilization of the solvent. Only one of the composition components can separate when the fibers are heated at high temperature in a furnace. Yang *et al.* [31] reported that PVP begins to decompose at 300°C and is destroyed when the furnace is heated up to 510°C. In this work, we introduce a new combined method to prepare PAN and PVP bended solvents to fabricate carbon nanofibers, in which ferromagnetism was observed. However, no works have yet been reported about ferromagnetic carbon material from PAN/PVP blends and furthermore, PVP polymer is cost effective. In considering the future potential of such materials, it is also necessary to take into account the lower costs of material.

In this work, it is clear that the ferromagnetic ordering in carbon nanofibers materials is highly dependent on the conditions of processing and the synthesis method adopted. Therefore, in light of this understanding, we systematically investigated the influence of the polyacrylonitrile and polyvinylpyrrolidone ratio on the structural, morphological, and magnetic properties of carbon nanofiber obtained. The PAN/PVP with a mass ratio of 10:0, 7:3, and 6:4 derived carbon nanofibers were fabricated by electrospinning and subsequent pyrolysis. Typical characterization techniques including X-ray diffraction (XRD), Raman spectroscopy (RS), Fourier transform infrared spectroscopy (FT-IR), field emission scanning electron microscopy (FE-SEM), and vibrating sample magnetometry (VSM). Furthermore, and importantly, X-ray photoelectron spectroscopy (XPS) was performed and contributed an important role in confirming and understanding in terms of bonding configuration of the carbon system and the contamination causing ferromagnetic behavior in the CNFs.

2. Experimental

2.1 Materials

Polyacrylonitrile (PAN, M_w =150,000), polyvinyl pyrrolidone (PVP, M_w =1,300,000) and N, N-dimethylformamide (DMF, 99.8%) were purchased from Sigma- Aldrich. All the materials were used without any further purification.

2.2 Fabrication of polymer nanofibers

The precursor solutions were prepared by dissolving polymer blends of PAN and PVP in three different weight ratios, 10:0, 7:3, and 6:4 in 40 ml

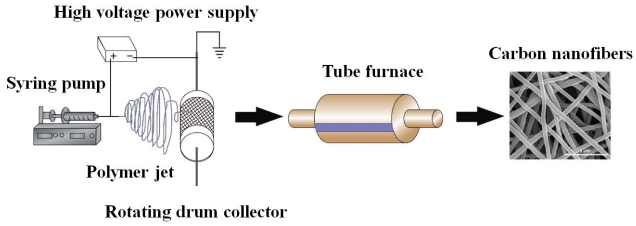

Figure 1. Schematic diagram setup for the electrospinning of carbon nanofibers.

of DMF. The mixed total mass of PAN and PVP in DMF was fixed to 10 wt% [32]. The PAN/PVP solutions were prepared with vigorous stirring for 5 h and ultrasonic-assisted vibration for 30 min until a homogeneous solution was obtained. Then, the solution mixture was transferred into a plastic syringe equipped with a 22-gauge needle made of stainless steel. The PAN or PAN/PVP electrospun fiber mats were prepared using a drum electrospinning process which is shown in Figure 1. The voltage used for electro-spinning was maintained between 15.6 kV to 16.0 kV. The distance between the syringe needle tip and the aluminum foil collector was set at 15 cm. The solution was fed at a flow rate of 0.5 mL·h^{-1}. The collection of electrospun fibers was set to 6 h. All as-spun fibers were stored at room temperature.

2.3 Pyrolysis of carbon nanofibers

Carbon nanofibers were obtained after completing the pyrolysis of polymer fibers. Fibers were subsequently placed inside a tube furnace for further processing to enable stabilization, carbonization, and additional activation. The carbon nanofibers obtained after pyrolysis of polymer fibers were placed inside a tube furnace and subjected to a three step process involving stabilizing at 280°C for 2 h in an air atmosphere at the heating rate of 2°C·min^{-1}, and then carbonized at 800°C for 2 h in an argon atmosphere at the heating rate of 5°C·min^{-1}. The activation was carried out through an increase in the temperature at rate of 5°C·min to at 800°C and the maintenance of the samples at this temperature for 2 h in an argon atmosphere. Finally, the carbonized nanofibers were activated by CO_2 ambience at 800°C for 30 min directly after carbonization.

2.4 Characterizations

The carbonization samples were characterized for crystal phase identification by XRD (Advance Bruker D8, Germany) with Cu-Kα radiation (λ=0.15406 nm). The morphology and average diameter of carbonization samples were characterized by FE-SEM (Helios Nanolab G3 CX). The chemical bonding and elemental composition of CNFs were analyzed by XPS (ULVAC-PHI, Japan) with Al K (1486.4 eV) radiation as the excitation source. The functional groups were characterized by FT-IR (Bruker Tensor 27, U.K). Characterization of the crystalline perfection of graphite- based samples employed Raman spectroscopy (Bruker, MultiRAM and SENTERRA II, UK). The magnetic measurements were investigated at room-temperature using a vibration sample magnetometer (Versalab^{TM} Tesla VSM 7403, USA).

3. Results and discussion

The morphology of nanofibers was analyzed by FE-SEM. Figure 2(a-c) shows the morphology of the as-spun pure PAN nanofibers, PAN/PVP (7:3) and PAN/PVP (6:4) obtained after electrospinning. The average diameter of nanofibers could be measured and calculated by the ImageJ software and Microsoft Excel. It was clear that all samples exhibited a smooth surface and were continuous cylindrical structures. Increasing the amount of PVP in the composites increased the average diameter between 474 nm to 740 nm. The average diameter of samples was found to decrease with increasing the PVP content because PVP completely degrades during the carbonization process. Figure 2(d), 2(e) and 2(f) show the morphology of the pure PAN nanofibers, PAN/PVP (7:3) and PAN/PVP (6:4) obtained after carbonization at 800°C; their diameters were 511±81 nm, 440±63 nm,

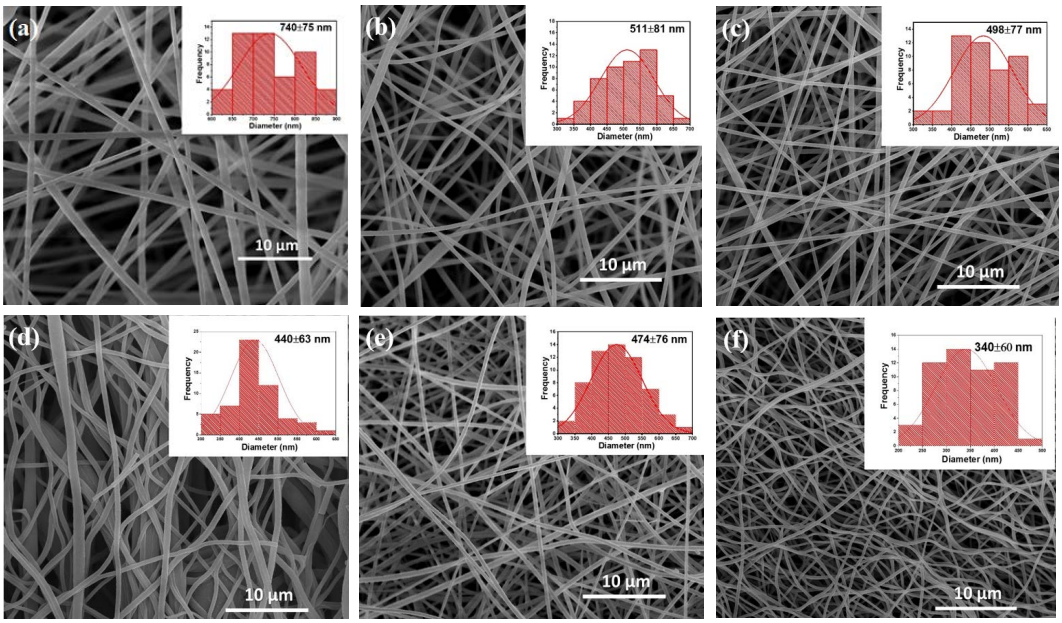

Figure 2. FE-SEM image of as-spun (a) PAN (b) PAN/ PVP (7:3) (c) PAN/ PVP (6:4) and after carbonized. (d) PAN (e) PAN/ PVP (7:3) and (f) PAN/ PVP (6:4).

and 340±60 nm, respectively. This average diameter was measured just on the fibrous morphology, it was not measured in interconnection areas. The reduction in average diameter of the nanofibers after calcination could be attributed to the loss of PVP and PAN from the nanofibers [32,36,37]. However, the size of fibers could be increased with the PVP content because of fiber-fiber interconnection. Niu *et al.* [38] reported that fiber diameter increased with the PAN/ PVP ratio at 13:87 and 8:92. There was almost no fiber – fiber interconnection at a low PVP content. In this case the interconnection fiber was formed only in small areas, which were mostly invisible, explaining why the fiber diameter decreased with the PVP content.

Figure 3 shows the XRD pattern of all samples used for investigation of their crystal structures. For all samples, diffraction peaks corresponding to the (002) and (101) peaks of graphitic carbon were observed at approximately 2θ = 25° and 44° [39]. The broad diffraction peaks suggest the disorder and amorphous characteristics of the materials [40]. These results imply that the crystal structure of PAN and PAN/ PVP nanofibers is not changed by increasing PVP content; only the intensity is changed, which in the sample PAN/PVP (6:4) is the lowest intensity and agrees with the previous report by Lv *et al.* [41]. This may result from the incorporation of carbon nanoparticles from PVP into the sample. The decrease in terms of diffraction peaks led to a decrease of degree of crystallinity of PAN/PVP nanofiber [42], but it was far from the perfect graphitized structure [43].

The surface elemental composition and their binding energies of samples were investigated XPS. The main peak contained two distinct peaks, indicating the existence of carbon, oxygen, and nitrogen elements, while nitrogen content in PAN/PVP (6:4) was a minority as shown in Figure 4. From the survey spectra, the intensity of O1s peak of PAN/PVP (6:4) sample was much stronger compared to the O1s of PAN. This result obviously indicated the increased oxygen functional groups in PAN/PVP (6:4). Figure 5(a-c) shows that the high-resolution C1s spectrum in all samples which can be deconvolved into three peaks centered; firstly, attributed to C-C and/or C=C [44-46] that originated from the sp^2 C-C bond, the relative intensity ratios of C-C/C=C for PAN, PAN/PVP(6:4), and PAN/PVP (7:3) were 78.97%, 75.66%, and 70.3%, respectively.; secondly C–O and/ or C-OH ranging 286.0 eV to 286.7 eV, the relative intensity ratios of C-O/C-OH for PAN, PAN/PVP(6:4), and PAN/PVP (7:3) were 11.67%, 18.50%, and 18.78%, respectively and lastly O–C=O and/

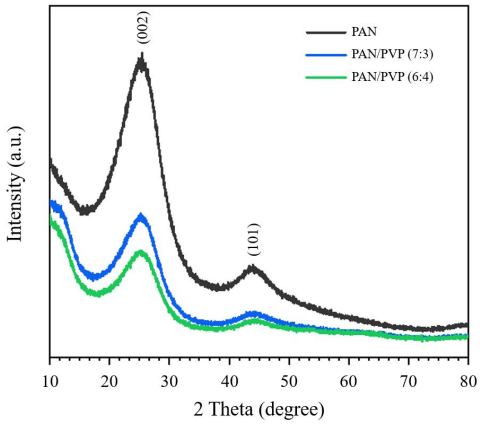

Figure 3. XRD patterns of carbon nanofiber from PAN and PAN mixed PVP in different ratio after carbonized.

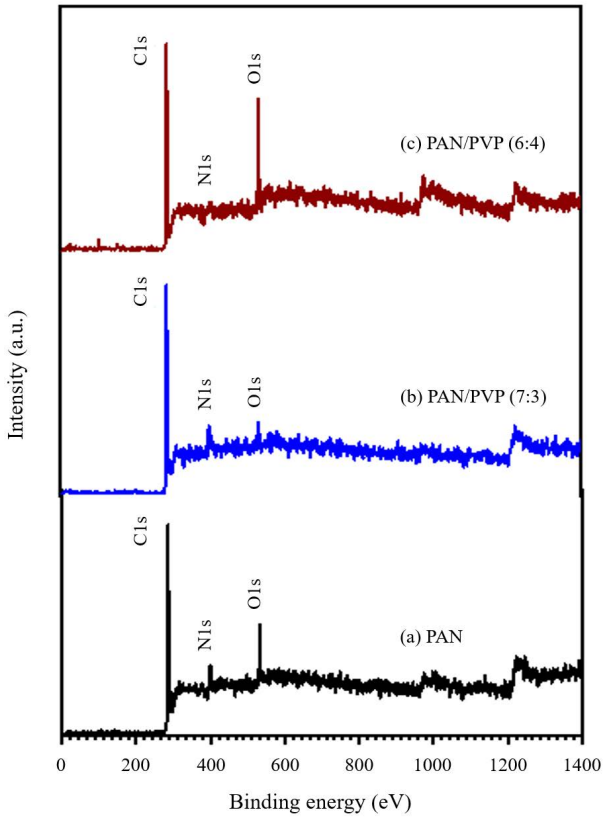

Figure 4. XPS survey spectra of carbon nanofiber from PAN and PAN mixed PVP (a) PAN (b) PAN/ PVP (7:3) and (c) PAN/ PVP (6:4) in different ratio carbonized nanofibers.

or O=C-NH ranging 287.6 eV to 289.5 eV [47], the relative intensity ratios of O-C=O/O=C-NH for PAN, PAN/PVP(6:4), and PAN/PVP (7:3) were 9.36%, 5.84%, and 10.94%, respectively. The results show the comparison of C-C/C=C, C-O-C and O-C=O of PAN, PAN/ PVP (7:3), and PAN/ PVP (6:4) (see Figure 5(d), 5(e), and 5(f). Notably, PAN/PVP (7:3) had the highest intensity ratio of O-C=O and peak position shifted towards higher binding energy, which involved the conductivity on the surface due to the local chemical of the neighboring atoms [32,48]. The O1s spectra of all samples deconvolved into two main peaks attributed to C=O and ranging from 531.1 eV to 531.8 eV and C–O ranging 532.4 eV to 533.2 eV (see Figure 6(a), 6(b), and 6(c) [36]. The comparison of C=O and C-O in all samples is shown in Figure 6(d) and 6(e).

The FT-IR spectra was generated in order to understand the relevant functional groups after the heat treatment activity. For comparison, pure PAN and PAN/PVP showed the absorption peak in Figure 7. The FT-IR spectra showed that the PVP could not change the functional groups in the samples, the appearance is similarity; however, a small shift in PAN/PVP (6:4) towards a higher wavenumber was observed and may have been due to the incorporation of carbon nanoparticles in the template. The broad absorption band at ~ 1160 cm^{-1} represents the stretching mode of C-O from the carboxyl group (-COOH) [49]. The peak at 1563 cm^{-1} represents the stretching mode of the C=C group from an aromatic ring [50,51]. The band at ~ 1800 cm^{-1} may be assigned to the C=O bond stretching vibration mode [52-54]. The peak at 1892 cm^{-1} was assigned to the aromatic combination band [55]. The peak around 2082 cm^{-1} indicates C≡C bending [56].

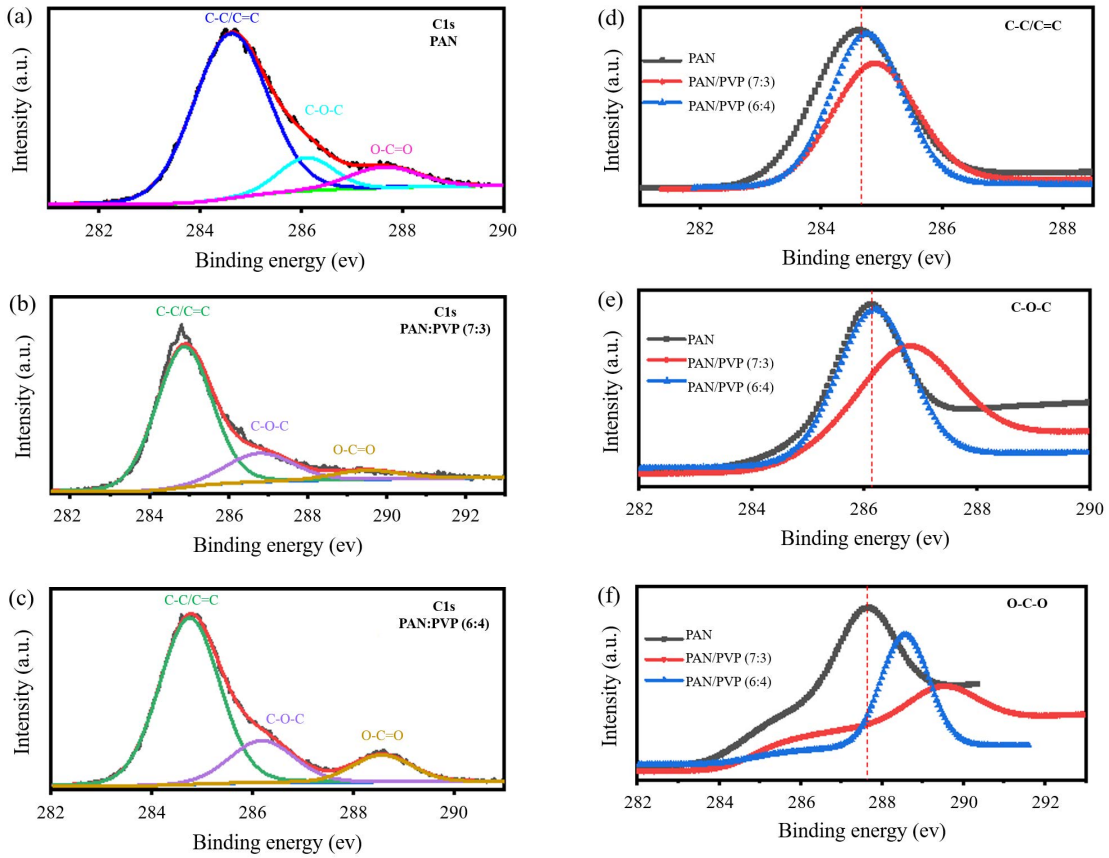

Figure 5. XPS C1s spectra and fitted curves of carbon nanofiber from PAN and PAN mixed PVP (a) PAN (b) PAN/ PVP (7:3) (c) PAN/ PVP (6:4) in different ratio carbonized nanofibers. The proportion for comparison of (d) C-C/C=C (e) C-O-C and (f) O-C=O in PAN, PAN/ PVP (7:3) and PAN/ PVP (6:4).

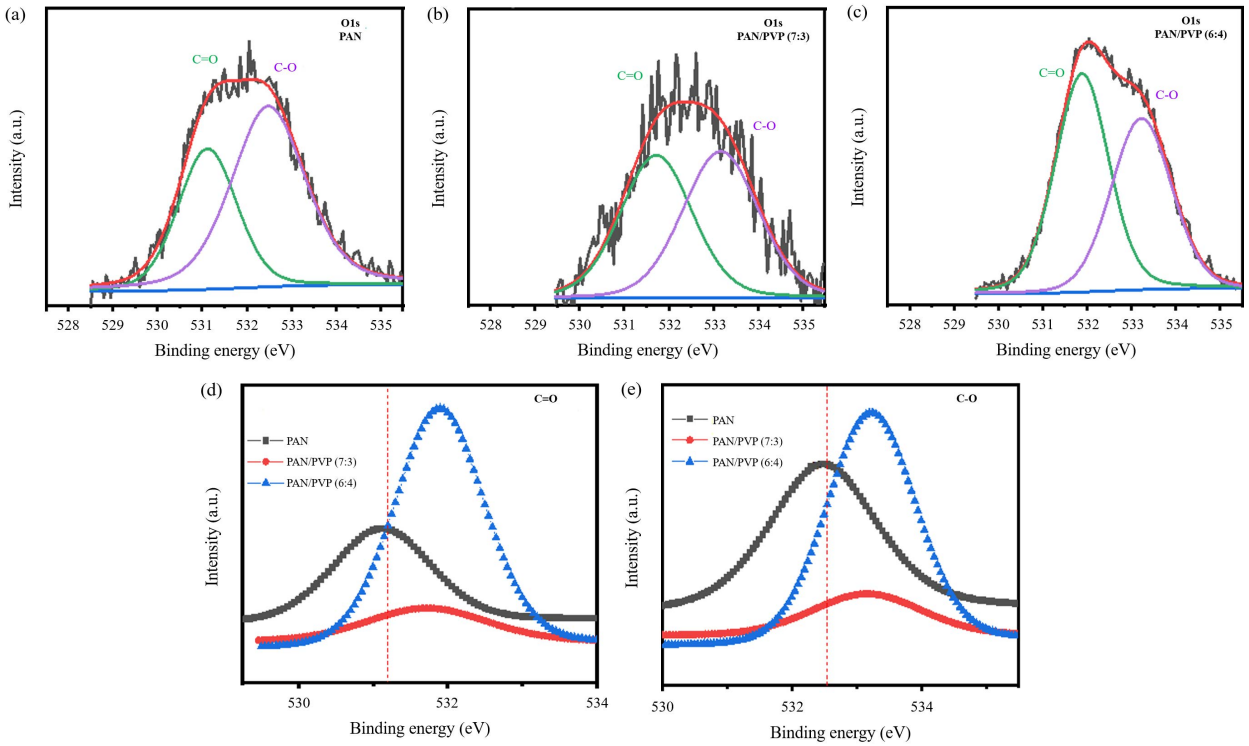

Figure 6. XPS O1s spectra and fitted curves of carbon nanofiber from PAN and PAN mixed PVP (a) PAN (b) PAN/ PVP (7:3) and (c) PAN/ PVP (6:4) in different ratio carbonized nanofibers. The proportion for comparison of (d) C=O and (e) C-O in PAN, PAN/ PVP (7:3) and PAN/ PVP (6:4).

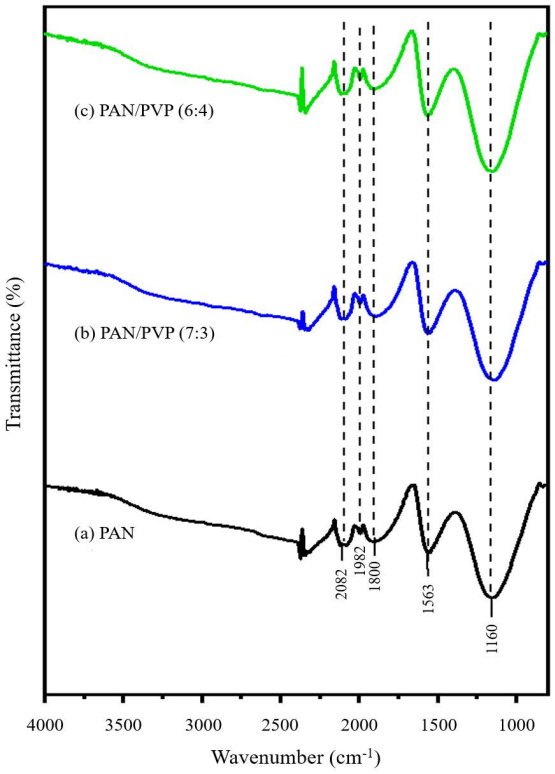

Figure 7. FT-IR spectra of carbon nanofiber from PAN and PAN mixed PVP (a) PAN (b) PAN/ PVP (7:3) and (c) PAN/ PVP (6:4) in different ratio carbonized nanofibers.

Raman analysis was used to determine the carbon quality of PAN and PAN/PVP (6:4) samples by using a Gaussian fitting of the observed band positions. In addition, Raman spectroscopy is a commonly used technique for identifying a secondary phase in doped/composites materials. The first-order zone boundary phonon mode component with D and G band, D band has sp^3 carbon bonded (C-C), associated with the disorder that was induced by defects (vacancies) in the carbon nanofibers. The G band results from the stretching of the C=C bonds in the hexagonal ring of sp^2 bonded carbon in graphitic structures [40,57]. Figures 8(a) and 8(b) show the D bands of the PAN and PAN/PVP (6:4) samples which are located at 1361.2 and 1359.9 cm^{-1} respectively. The G band showed peaks at 1580.5 cm^{-1} and 1581.8 cm^{-1} that corresponded to an ideal graphitic lattice vibration mode of E_{2g} symmetry [58]. The intensity ratio of D band to G band ($R=I_D/I_G$) reflects to the degree of the defects in the carbon nanofibers. This work showed an I_D/I_G ratio value at 1.78 for the PAN sample which was obtained from the peaks in Figure 8(a). The I_D/I_G value of carbon nanofibers increased to 1.89 with decreasing ratio of PAN/PVP (6:4) (see Figure 8(b)). A comparison of the spectra of PAN and PAN/ PVP (6:4) is shown in Figure 8(c). An increase in the I_D/I_G ratio indicates an increase in the number of defects on nanofibers, which indicates the decrease in the average diameter size, in agreement with the FE-SEM result [51]. The observed Raman bands around 2704 cm^{-1} and 2870 cm^{-1} were assigned to the secondary order zone boundary phonon mode component that related to the phonon oscillation in the infinite crystal of graphite structure for the samples of PAN and PAN/PVP (6:4), respectively [59]. No additional peaks of impurities are observed in the spectrum. From, the information of surface functional groups obtained by XPS, FT-IR and Raman, the result suggested agreement in C=O, C-O and C≡C. The result indicated that the surface of carbon nanofibers contained C-C/C=C, C-O, and C=O.

The specific saturation magnetization (M–H curves) of PAN and PAN/PVP carbon nanofibers were obtained at room temperature. The VSM measurement in Figure 9(a-d) shows that the magnetic hysteresis loops with applied magnetic field cycled between -15000 Oe and 15000 Oe. The samples exhibited magnetic behavior after subtracting the diamagnetic contribution from the gel cap sample holder. The M-H curve of all samples was representative for a magnetic material and indicated hysteresis in ferromagnetic component in the field ranges of ±5000 Oe; while outside this range, the specific saturation magnetization slightly increases with increasing field. The specific saturation magnetization values of 34.7, 7.7, and 144.2 m-emu·g^{-1} and coercivity of 949.6, 1763.5 and 2777.0 Oe were observed for the PAN, PAN/PVP (7:3) and PAN/PVP (6:4) samples, respectively (Table 1). The coercivity is the demagnetizing field needed to reduce the remnant magnetization to zero [60]. This study shows that the coercivity values of samples increased with average fiber diameter and the increase of oxygen functional groups attached on the surface. The ferromagnetic component increases in an unusual manner related to increasing the content of PVP in samples, when the increasing PAN in composite leads to a decrease in magnitude of the specific saturation magnetization. According to our XPS results, the C:O ratios of the PAN, PAN/PVP (7:3) and PAN/PVP (6:4) were 87.95:12.05, 92.98:7.02 and 89.78:10.22, respectively. In addition, as can be noticed, the percentage proportion of O-C=O bonds in all PAN/PVP ratios may correlate with the change in their magnetization, which affects the electrical conductivity of them. The oxygen coverage was small in PAN/PVP (7:3) so that it was possible for magnetic ordering to occur because the magnetic domain could develop in graphite oxide [61], while increasing of PAN/PVP (6:4) lead to an increase in a specific saturation magnetization of content that shows the highest magnetic moment of our sample. This may be due to increasing amorphization that correlated with the increasing ratio of I_D/I_G from Raman analysis. The I_D/I_G monotonically increased with the PVP content, which indicates an increased density of vacancy defects [6]. The results show that the amount of vacancy in samples tends to increase with PVP content. The vacancy in samples is predicted to have local magnetic moments [62]. The local moments could couple each other and produce a long-range order, and could give rise to ferromagnetic behavior in samples, which explained the increase in the magnetization in the PAN/PVP (6:4) sample. Furthermore, the carbon atoms neighboring to defects in samples will adjust their bonds to accommodate the defects and produce dangling sp^2 bonds, which generate a magnetic moment. Thus, we suggest that the origin of the ferromagnetism be attributed to the mixture of carbon atoms with sp^2 and sp^3 bonds according to the above XPS and Raman analysis, and this creates vacancies in the presence of unpaired electron spins in sp^3 carbon bonds that contribute the ferromagnetism [7,63]. In addition, the FE-SEM showed the smallest average diameter of nanofibers were possible magnetically ordered due to the large amount of graphitized carbons edge sites magnetism [18,64]. The observed ferromagnetism could be based on the rich carbon defects of carbon dangling bonds and strong ferromagnetic coupling between them [3]. This suggest that the increasing disorder in the graphite structure in

samples clearly played an important role in improving the ferromagnetic properties of graphite, in agreement with the results of the ratio of I_D/I_G [60]. This observation is consistent with previous research results of Saito *et al.* [8] reported that the carbon material prepared by pyrolysis of PAN at 1273 K for 1 h exhibits a saturation magnetization of 1.22 emu·g^{-1} at 300 K.

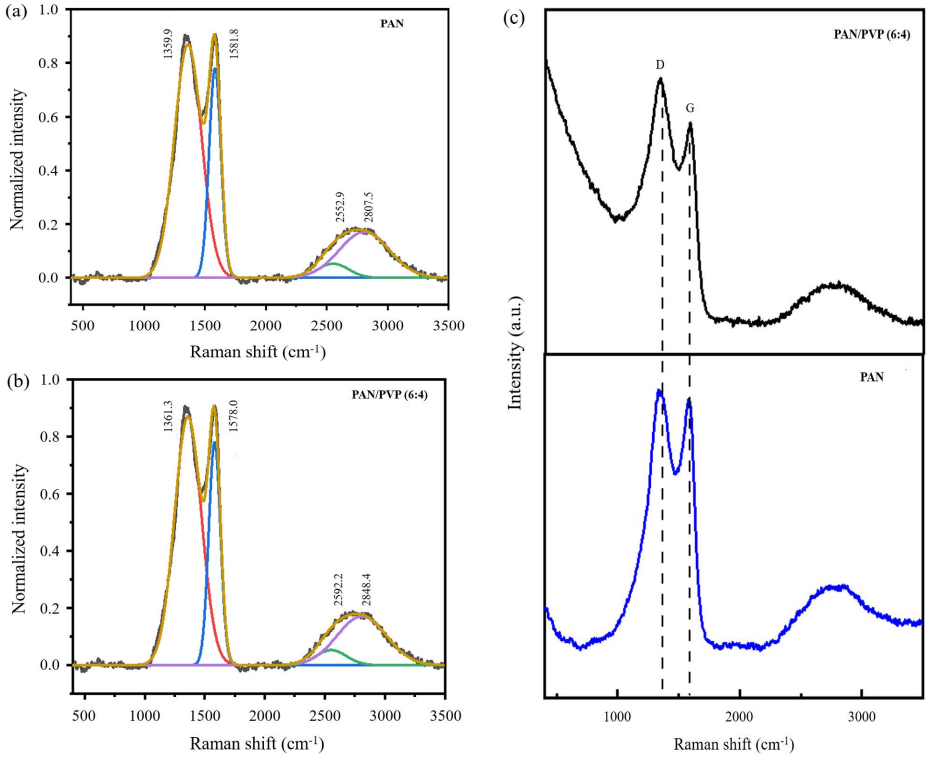

Figure 8. Raman Fitting curves of carbon nanofiber carbonized nanofibers. (a) PAN and (b) PAN/PVP (6:4). Raman spectra of (c) PAN and PAN/PVP (6:4).

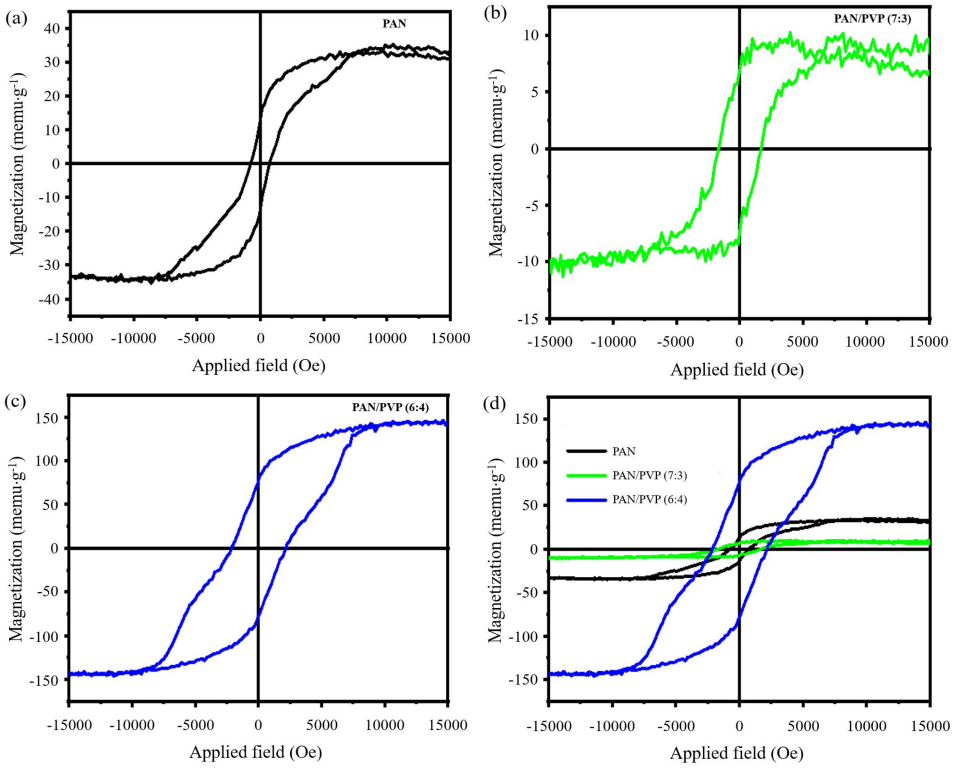

Figure 9. Magnetization of carbon nanofiber from PAN, PAN/PVP (7:3) and PAN/ PVP (6:4) in different ratio carbonized nanofibers as a function of field at 300 K.

Table 1. The magnetization and coercivity of carbon nanofiber from PAN and PAN/ PVP blend for different concentration.

Samples	Average diameter (nm)	Magnetization, M_s ($memu \cdot g^{-1}$)	Coercivity, H_c (Oe)
PAN	511±81	34.7	949.6
PAN/PVP (7:3)	440±63	7.7	1763.5
PAN/PVP (6:4)	340±60	144.2	2777.0

4. Conclusions

In conclusion, we report the existence of room-temperature ferromagnetism in carbon nanofibers without any transition metal in them. Carbon nanofibers were fabricated using electrospinning followed by pyrolysis. The observed ferromagnetism in samples can be described by the mixed fraction of sp^2 and sp^3 carbon atoms in carbon nanofibers; furthermore, the nanostructure could also play an important role in the net magnetic moment obtained. Further optimization of the temperature pyrolysis process and type of polymer may be needed to achieve a further increase in the saturation magnetization of material. This finding suggests an inexpensive method for preparing magnetic particles and human-friendly ways to produce magnetic material without metals, which can be applied in magnetic shielding or biocompatibility. This will aid the development of new technologies in the near future.

References

[1] J. M. D. Coey, "d^0 Ferromagnetism," *Solid State Sciences*, vol. 7, no. 6, pp. 660-667, 2005.

[2] A. Goldman and A. Goldman, "Applications and Functions of Ferromagnetic Materials," in *Handbook of Ferromagnetic Materials*, Kluwer Academic Publishing, 1999, pp. 1-15.

[3] X. L. Wu, R. S. Wang, J. Cheng, G. H. Zhong, X. J. Chen, Y. Gao, and Z. B. Huang, "Room temperature ferromagnetism in naphthalene," *Carbon,* vol. 36, pp. 125-129, 2018.

[4] P. Esquinazi and R. Höhne, "Magnetism in carbon structures," *Journal of Magnetism and Magnetic Materials*, vol. 290-291, pp. 20-27, 2005.

[5] R. Caudillo, X. Gao, R. Escudero, M. José-Yacaman, and J. B. Goodenough, "Ferromagnetic behavior of carbon nanospheres encapsulating silver nanoparticles," *Physical Review B: Condensed Matter and Materials Physics*, vol. 74, no. 21, pp. 1-12, 2006.

[6] Z. He, H. Xia, X. Zhou, X. Yang, Y. Song, and T. Wang, "Raman study of correlation between defects and ferromagnetism in graphite," *Journal of Physics D: Applied Physics*, vol. 44, no. 8, pp. 1-9, 2011.

[7] J. Červenka, M. I. Katsnelson, and C. F. J. Flipse, "Room-temperature ferromagnetism in graphite driven by two-dimensional networks of point defects," *Nature Physics*, vol. 5, no. 11, pp. 840-844, 2009.

[8] T. Saito, D. N. Hamane, S. Yoshii, and T. Nojima, "Ferromagnetic carbon materials prepared from polyacrylonitrile," *Applied Physics Letters*, vol. 98, no. 5, pp. 12-15, 2011.

[9] H. Pardo, N. D. Khan, R. Faccio, F. M. A. Moreira, L. F. Werner, T. Makarova, and Á.W. Mombrú, "Raman characterization of bulk ferromagnetic nanostructured graphite," *Physica B: Condensed Matter*, vol. 407, no. 16, pp. 3206-3209, 2012.

[10] S. S. Rao, S. N. Jammalamadaka, A. Stesmans, V. V. Moshchalkov, J. V Tol, D. V. Kosynkin, A. H. Duque, and J. M. Tour, "Ferromagnetism in graphene nanoribbons: Split versus oxidative unzipped ribbons," *Nano Letters*, vol. 12, no. 3, pp. 1210-1217, 2012.

[11] P. Esquinazi, D. Spemann, R. Höhne, A. Setzer, K. H. Han, and T. Butz, "Induced magnetic ordering by proton irradiation in graphite," *Physical Review Letters*, vol. 91, no. 22, pp. 8-11, 2003.

[12] X. Yang, H. Xia, X. Qin, W. Li, Y. Dai, X. Liu, Y. Xia, S. Yan, and B. Wang, "Correlation between the vacancy defects and ferromagnetism in graphite," *Carbon*, vol. 47, no. 5, pp. 1399-1406, 2009.

[13] S. Okada, K. Nakada, K. Kuwabara, K. Daigoku, and T. Kawai, "Ferromagnetic spin ordering on carbon nanotubes with topological line defects," *Physical Review B: Condensed Matter and Materials Physics*, vol. 74, no. 12, pp. 2-5, 2006.

[14] Z. Zanolli and J. C. Charlier, "Spin transport in carbon nanotubes with magnetic vacancy-defects," *Physical Review B: Condensed Matter and Materials Physics*, vol. 81, no. 16, 2010.

[15] U. Weissker, S. Hampel, A. Leonhardt, and B. Büchner, "Carbon nanotubes filled with ferromagnetic materials," *Materials (Basel)*, vol. 3, no. 8, pp. 4387-4427, 2010.

[16] H. Ohldag, T. Tyliszczak, R. Höhne, D. Spemann, P. Esquinazi, M. Ungureanu, and T. Butz, "Π-Electron Ferromagnetism in Metal-Free Carbon Probed by Soft X-Ray Dichroism," *Physical Review Letters*, vol. 98, no. 18, 2007.

[17] S. Talapatra, P. G. Ganesan, T. Kim, R. Vajtai, M. Huang, M. Shima, G. Ramanath, D. Srivastava, S. C. Deevi, and P. M. Ajayan, "Irradiation-induced magnetism in carbon nanostructures," *Physical Review Letters*, vol. 95, no. 9, 2005.

[18] A. Komlev, E. Lähderanta, E. Shevchenko, and N. Vorob'ev-Desyatovskii, "Magnetism of purified amorphous carbon," *EPJ Web of Conferences,* vol. 185**,** pp. 8-11, 2018.

[19] Y. W. Ma, Y. H. Lu, J. B. Yi, Y. P. Feng, T. S. Herng, X. Liu, D. Q. Gao, D. S. Xue, J. M. Xue, J. Y. Ouyang, and J. Ding, "Room temperature ferromagnetism in Teflon due to carbon dangling bonds," *Nature Communications*, vol. 3, 2012.

[20] E. Lähderanta, A. V. Lashkul, K. G. Lisunov, D. A. Zherebtsov, D. M. Galimov, and A. N. Titkov, "Magnetic properties of carbon nanoparticles," *IOP Conference Series: Materials Science and Engineering,* vol. 38, no. 1, pp. 1-7, 2012.

[21] G. Z. Magda, X. Jin, I. Hagymási, P. Vancsó, Z. Osváth, P. N. Incze, C. Hwang, L. P. Biró, and L. Tapasztó," Room-temperature magnetic order on zigzag edges of narrow graphene nanoribbons," *Nature*, vol. 514, no. 7524, pp. 608-611, 2014.

[22] P. O. Lehtinen, A. S. Foster, A. Ayuela, A. Krasheninnikov, K. Nordlund, and R. M. Nieminen, "Magnetic Properties and

Diffusion of Adatoms on a Graphene Sheet," *Physical Review Letters*, vol. 91, no. 1, pp.1-4, 2003.

[23] Y. Zhang, S. Talapatra, S. Kar, R. Vajtai, S. K. Nayak, and P. M. Ajayan, "First-principles study of defect-induced magnetism in carbon," *Physical Review Letters*, vol. 99, no. 10, pp. 1-4, 2007.

[24] O. V. Yazyev, and L. Helm, "Defect-induced magnetism in graphene," *Physical Review B: Condensed Matter and Materials Physics*, vol. 75, no. 12, pp. 1-5, 2007.

[25] P. Esquinazi, A. Setzer, R. Hoehne, C. Semmelhack, Y. Kopelevich, D. Spemann, T. Butz, B. Kohlstrunk, and M. Loesche, "Ferromagnetism in oriented graphite samples," *Physical Review B: Condensed Matter and Materials Physics*, vol. 66, no. 2, pp. 1-10, 2002.

[26] A. A. Ovchinnikov and V. N. Spector, "Organic ferromagnets. New results," *Synthetic Metals,* vol. 27, no. 3-4, pp. 615-624, 1988.

[27] C. Liu, Y. Yang, Z. Ma, C. Zhou, D. Liu, X. Luo, X. Zhu, Y. Sun, and Z. Sheng, "Edge-Induced Room-Temperature Ferromagnetism in Carbon Nanosheets," *The Journal of Physical Chemistry C*, vol. 124, pp. 7396-7403, 2020.

[28] J. J. P. Barragán, K. Gross, H. A. Calderón, P. Prieto, C. D. Giorgio, F. Bobba, and A. M. Cucolo, "Room-temperature ferromagnetism in oxidized-graphenic nanoplatelets induced by topographic defects," *Journal of Magnetism and Magnetic Materials*, vol. 524, pp. 664-674, 2021.

[29] J. C. Ruiz-cornejo, "Synthesis and applications of carbon nanofibers: a review," *Reviews in Chemical Engineering*, vol. 36, no. 4, pp. 1-19, 2018.

[30] S. Hao, V. L. J. Joly, S. Kaneko, and J. Takashiro, "Magnetic edge-states in nanographene, HNO_3-doped nanographene and its residue compounds of nanographene-based nanoporous carbon," *Physical Chemistry Chemical Physics*, vol. 16, pp. 6273-6282, 2014.

[31] K. S. Yang, D. D. Edie, D. Y. Lim, Y. M. Kim, and Y. O. Choi, "Preparation of carbon fiber web from electrostatic spinning of PMDA-ODA poly (amic acid) solution," *Carbon*, vol. 41, pp. 2039-2046, 2003.

[32] G. H. An, B. R. Koo, and H. J. Ahn, "Activated mesoporous carbon nanofibers fabricated using water etching-assisted templating for high-performance electrochemical capacitors," *Physical Chemistry Chemical Physics*, vol. 18, no. 9, pp. 6587-6594, 2016.

[33] M. Samadishadlou, M. Farshbaf, N. Annabi, T. Kavetskyy, R. Khalilov, S. Saghfi, A. Akbarzadeh, and S. Mousavi, "Magnetic carbon nanotubes: preparation, physical properties, and applications in biomedicine," *Artificial Cells, Nanomedicine and Biotechnology*, vol. 46, no. 7, pp. 1314-1330, 2018.

[34] K. E. Albinali, M. M. Zagho, Y. Deng, and A. A Elzatahry, "A perspective on magnetic core – shell carriers for responsive and targeted drug delivery systems," *International Journal of Nanomedicine*, vol. 14, pp. 1707-1723, 2019.

[35] T. L. Makarova, "Ferromagnetic Carbonaceous Compounds," in *Carbon Based Magnetism*, Elsevier, 2006, pp. 541-562.

[36] D. Xiang, X. Liu, and X. Dong, "A facile synthetic method and electrochemical performances of nickel oxide/carbon fibers composites," *Journal of Materials Science*, vol. 52, no. 13, pp. 7709-7718, 2017.

[37] X. Zhou, Y. Wang, C. Gong, B. Liu, and G. Wei, "Production, structural design, functional control, and broad applications of carbon nano fiber-based nanomaterials: A comprehensive review," *Chemical Engineering Journal,* vol. 402, pp. 126189, 2020.

[38] H. Niu, J. Zhang, Z. Xie, X. Wang, and T. Lin, "Preparation, structure and supercapacitance of bonded carbon nanofiber electrode materials," *Carbon*, vol. 49, no. 7, pp. 2380-2388, 2011.

[39] O. Pech, and S. Maensiri, "Electrochemical performances of electrospun carbon nanofibers, interconnected carbon nanofibers, and carbon-manganese oxide composite nanofibers," *Journal of Alloys and Compounds*, vol.781, pp. 541-552, 2019.

[40] S. Ma, J. H. Xia, V. V. S. S. Srikanth, X. Sun, T. Staedler, X. Jiang, F. Yang, and Z. D. Zhang, "Magnetism of amorphous carbon nanofibers," *Applied Physics Letters*, vol. 95, pp. 1-4, 2009.

[41] J. Lv, W. Gu, X. Cui, S. Dai, B. Zhang, and G. Ji, "Nanofiber network with adjustable nanostructure controlled by PVP content for an excellent microwave absorption," *Scientific Reports*, vol. 9, no. 1, pp. 2-11, 2019.

[42] O. M. Mpukuta, K. Dincer, and M. O. Erdal, "Investigation of electrical conductivity of PAN nanofibers containing silica nanoparticles produced by electrospinning method," *Materials Today: Proceedings*, vol. 18, pp. 1927-1935, 2019.

[43] G. Wanga, C. Panab, L. Wanga, Q. Donga, C. Yua, Z. Zhaoa, and J. Qiu, "Activated carbon nanofiber webs made by electro-spinning for capacitive deionization," *Electrochimica Acta*, vol. 69**,** pp. 65-70, 2012.

[44] Z. Yue, K. R. Benak, J. Wang, C. L. Mangun, and J. Economy, "Elucidating the porous and chemical structures of $ZnCl_2$-activated polyacrylonitrile on a fiberglass substrate," *Journal of Materials Chemistry*, vol. 15, no. 30, pp. 3142-3148, 2005.

[45] L. Pérez-Álvarez, L. Ruiz-Rubio, I. Moreno, and J. L. Vilas-Vilela, "Characterization and optimization of the alkaline hydrolysis of polyacrylonitrile membranes," *Polymers (Basel)*, vol.11, no. 11, pp.1-11, 2019.

[46] B. Xu, S. Yue, Z. Sui, X. Zhang, S. Hou, G. Cao, and Y. Yang, "What is the choice for supercapacitors: Graphene or graphene oxide," *Energy & Environmental Science*, vol. 4, no. 8, pp. 2826-2830, 2011.

[47] E. N. Attia, F. M. Hassan, M. Li, R. Batmaz, A. Elkamel, and Z. Chen, "Tailoring the chemistry of blend copolymers boosting the electrochemical performance of Si-based anodes for lithium ion batteries," *Journal of Materials Chemistry A*, vol. 5, no. 46, pp. 24159-24167, 2017.

[48] D. R. Baer, K. Artyushkova, H. Cohen, C. D. Easton, M. Engelhard, T. R. Gengenbach, G. Greczynski, P. Mack, D. J. Morgan, and A. Roberts, "XPS guide: Charge neutralization and binding energy referencing for insulating samples XPS guide: Charge neutralization and binding energy referencing for insulating samples," *Journal of Vacuum Science and Technology A*, vol. 38, no. 3, pp. 1-19, 2020.

[49] V. Ţucureanu, A. Matei, and A. M. Avram, "FTIR Spectroscopy for Carbon Family Study," *Critical Reviews in Analytical Chemistry*, vol. 46, no. 6, pp. 502-520, 2016.

[50] A. C. Obreja, D. Cristea, R. Gavrila, V. Schiopu, A. Dinescu, M. Danila, and F. Comanescu, "Isocyanate functionalized

graphene/P3HT based nanocomposites," *Applied Surface Science*, vol. 276, pp. 458-467, 2013.

[51] C. Liu, and K. Lafdi, "Fabrication and characterization of carbon nanofibers from polyacrylonitrile/pitch blends," *Journal of Applied Polymer Science*, vol. 134, no. 42, pp. 1-7, 2017.

[52] N. B. A. Mansor, J. P. Tessonnier, A. Rinaldi, S. Reiche, and M. G. Kutty, "Chemically modified multi-walled carbon nanotubes (MWCNTs) with anchored acidic groups," *Sains Malaysiana*, vol. 41, no. 5, pp. 603-609, 2012.

[53] V. A. E. Barrios, J. R. R. Méndez, N. V. P. Aguilar, G. A. Espinosa, and J. L. D. Rodríguez, "FTIR - An Essential Characterization Technique for Polymeric Materials," in Infrared Spectroscopy - Materials Science, Engineering and Technology, ed Greece, 2012, pp. 195-210.

[54] M. R. Johan, S. H. Meriam Suhaimy, and Y. Yusof, "Physico-chemical studies of cuprous oxide (Cu_2O) nanoparticles coated on amorphous carbon nanotubes (α-CNTs)," *Applied Surface Science*, vol. 289, pp. 450-454, 2014.

[55] J. Coates, "Interpretation of Infrared Spectra, A Practical Approach," in *Encyclopedia of Analytical Chemistry*, John Wiley & Sons, 2006, pp.1-23.

[56] F. E. C Othman, N. Yusof, J. Jaafar, A. F. Ismail, H. Hasbullah, N. Abdullah, and M. S. Ismail, "Preparation and characterization of Polyacrylonitrile/ Manganese Dioxides- based Carbon Nanofibers via electrospinning process," *IOP Conference Series: Earth and Environmental Science*, vol. 36, no. 1, pp. 012006, 2016.

[57] J. Yan, Q. Wang, T. Wei, and Z. Fan, "Recent advances in design and fabrication of electrochemical supercapacitors with high energy densities," *Advanced Energy Materials*, vol. 4, no. 4, pp. 1-43, 2014.

[58] A. Sadezky, H. Muckenhuber, H. Grothe, R. Niessner, and U. Pöschl, "Raman microspectroscopy of soot and related carbonaceous materials: Spectral analysis and structural information," *Carbon*, vol. 43, no. 8, pp. 1731-1742, 2005.

[59] M. A. Pimenta, G. Dresselhaus, M. S. Dresselhaus, L. G. Cançado, A. Jorio, and R. Saito, "Studying disorder in graphite-based systems by Raman spectroscopy," *Physical Chemistry Chemical Physics*, vol. 9, no. 11, pp. 1276-1291, 2007.

[60] R. N. Bhowmik, "Ferromagnetism in lead graphite-pencils and magnetic composite with $CoFe_2O_4$ particles," *Composites Part B: Engineering*, vol. 43, no. 2, pp. 503-509, 2012.

[61] D. Lee and J. Seo, "Magnetic frustration of graphite oxide," *Scientific Reports*, vol. 7, pp. 2-7, 2017.

[62] P. O. Lehtinen, A. S. Foster, Y. Ma, A. V. Krasheninnikov, and R. M. Nieminen, "Irradiation-induced magnetism in graphite: A density functional study," *Physical Review Letters*, vol. 93, no. 18, pp. 1-4, 2004.

[63] A. Sinha, A. Ali, and A. D. Thakur, "Ferromagnetism in graphene oxide," *Materials Today: Proceedings,* vol. 46, no. 14, pp. 6230-6233, 2021.

[64] T. Ishii, Y. Kaburagi, A. Yoshida, Y. Hishiyama, H. Oka, N. Setoyama, J. Ozaki, and T. Kyotani, "Analyses of trace amounts of edge sites in natural graphite, synthetic graphite and high-temperature treated coke for the understanding of their carbon molecular structures," *Carbon*, vol. 125, pp. 146-155, 2017.